RSC Advances

PAPER

View Article Online
View Journal | View Issue

Check for updates

Cite this: *RSC Adv.*, 2021, **11**, 16351

Whether planar or corrugated graphitic carbon nitride combined with titanium dioxide exhibits better photocatalytic performance?

Nguyen Thi Thu Ha,[a] Pham Thi Be,[ab] Phung Thi Lan,[a] Nguyen Thi Mo,[a] Le Minh Cam[a] and Nguyen Ngoc Ha*[a]

Received 15th February 2021
Accepted 18th April 2021

DOI: 10.1039/d1ra01237a

rsc.li/rsc-advances

The density functional theory method was performed to study the electronic structures of planar (pGN), corrugated (cGN) graphitic carbon nitride and their interactions with titanium dioxide cluster $(TiO_2)_7$. The transfer of photoinduced electrons was analyzed and electronic excitations were calculated. The obtained results show that cGN is thermodynamically more stable than pGN. cGN chemically interacts with titanium dioxide clusters, while the interaction between pGN and the cluster is assigned to physical nature. The combination of cGN and pGN with $(TiO_2)_7$ reduces the energy of the first excited states compared to that of the pure substances. The photocatalytic activities were estimated based on hypotheses on the location of the reduction and oxidation sites, the distance between the photoinduced holes and electrons and the electron density of molecular orbitals involved in the excitation. cGN/TiO_2 is predicted to have a higher photocatalytic activity than pGN/TiO_2.

Introduction

Graphitic carbon nitride (g-C_3N_4) is a relatively new type of carbon-based material that is being researched in the last few decades. g-C_3N_4 possesses many unique properties such as non-toxicity, high thermal and chemical stability, simplicity of fabrication techniques, moderate band gap, which make it a promising candidate in electronic, catalytic and energetic applications.[1,2] In particular since Wang and his co-workers first discovered the photocatalytic H_2 and O_2 evolution by water splitting over g-C_3N_4 in 2009,[3] g-C_3N_4 has gained tremendous attention as an organic semiconductor metal-free photocatalyst. Recently, g-C_3N_4 has been widely investigated for the photodegradation of organic pollutants,[4–6] water splitting,[7,8] CO_2 conversion,[9–11] *etc.* However, high electron–hole pair recombination rate and insufficient visible absorption are principal drawbacks of g-C_3N_4. Many efforts have been devoted to overcoming these two deficiencies by modifying the electronic band structure of g-C_3N_4 through methods such as metal ion doping,[12] non-metal doping,[13] noble metal-loading[9,14] or creating heterojunction structures with other semiconductors.[10,11,15,16] The latter has been shown to be an effective method for improving photocatalytic performance through better charge separation at the interface between two semiconductors since valence and conduction bands (VB and CB) of one semiconductor are located at higher energy levels compared to those of other coupling semiconductors. The popular semiconductor widely used for coupling with g-C_3N_4 is a traditional photocatalyst – titanium dioxide (TiO_2). The combination of g-C_3N_4 and TiO_2 (g-C_3N_4/TiO_2) has shown to exhibit higher photocatalytic activity compared to that of pure materials in many reactions due to the efficient separation of the photogenerated electron–hole pairs.[15,17–22] However, the inside mechanism of electron transfer in the g-C_3N_4/TiO_2 combination and the interaction between components are still rarely discussed in the literature. Wang *et al.* studied TiO_2–C_3N_4 hybrid microspheres[21] and found that this hybrid material exhibited superior photocatalytic activity compared to TiO_2–C_3N_4 composites prepared by traditional physical mixing methods. In the FTIR spectrum of the hybrid material, some location shifts of C_3N_4 characteristic bands were observed, suggesting the presence of chemical interaction or a synergistic effect between TiO_2 and C_3N_4. Fagan *et al.* studied photocatalytic properties of g-C_3N_4/TiO_2 heterojunctions[22] and reported a substantial up-field shift in Raman spectra upon the addition of g-C_3N_4 to TiO_2, indicating the formation of new bonds or bond modifications. Therefore, the authors suggested that g-C_3N_4 was probably incorporated into the TiO_2 system rather than existing as a component of the mixture of the two.[19]

The structural and optical properties of the g-C_3N_4/TiO_2 system have also been intensively investigated in various theoretical studies.[15,19,20,23,24] Lin *et al.* studied the electronic and optical properties of g-C_3N_4/TiO_2(101) heterostructure using

[a]Faculty of Chemistry, Hanoi National University of Education, 136 Xuan Thuy Str., Hanoi, Vietnam. E-mail: hann@hnue.edu.vn

[b]Faculty of Natural Science and Technology, Taynguyen University, Daklak, Vietnam

Open Access Article. Published on 05 May 2021. Downloaded on 2/10/2026 5:16:54 PM.
This article is licensed under a Creative Commons Attribution-NonCommercial 3.0 Unported Licence.

Open Access Article. Published on 05 May 2021. Downloaded on 2/10/2026 5:16:54 PM.
This article is licensed under a Creative Commons Attribution-NonCommercial 3.0 Unported Licence.

spin-polarized DFT+U calculations.[15] Based on the calculated equilibrium distance between g-C_3N_4 and anatase TiO_2(101) (1.94 Å) and the binding energy (24 meV $Å^{-2}$), the g-C_3N_4/TiO_2(101) composite material was assigned to the van der Waals heterostructure. The authors also noticed that the electrons can migrate from the g-C_3N_4 monolayer to anatase TiO_2 (101) surface, which leads to oxidation and redox reactions occurring on g-C_3N_4 and TiO_2, respectively. A similar charge transfer was reported in the work of Liu *et al.*[20] The interaction between TiO_2 and g-C_3N_4 results in the formation of a built-in electric field at the interface, which encourages the separation of electron–hole pairs.[15,19,20] Gao *et al.* suggested that electron transition from the highest occupied molecular orbital (HOMO) to the lowest unoccupied molecular orbital (LUMO) promoted the separation of electrons and holes.[19]

Obviously, the interaction between TiO_2 and g-C_3N_4 plays a crucial role in the photocatalytic performance of the combined material. It is also has been reported in various studies that the structure of the material, including deficient structures of g-C_3N_4, significantly influences its catalytic activity.[25–28] Lei *et al.* studied a TiO_2/g-C_3N_4 composite photocatalyst with an inverse opal structure and heterojunction[28] and showed that the inverse opal TiO_2/g-C_3N_4 degraded Rhodamine B 2.7 times faster than the normal TiO_2/g-C_3N_4, owing to the interaction between inverse opal g-C_3N_4 and TiO_2 creating more interfaces for the efficient transfer of photogenerated electron–hole pairs.[29] Ren *et al.* studied stabilities, electronic properties, and nitrogen reduction activity of planar and corrugated conformations of g-C_3N_4 (ref. 25) and showed the distortion conformation could activate more n → π* transitions of g-C_3N_4, promoting separation efficiency of photoinduced carriers in g-C_3N_4. The stability of the corrugated geometry of g-C_3N_4 compared to the planar geometry was highlighted in several theoretical studies. The corrugation was proved to minimize the electronic repulsion experienced by the N lone pairs located in their structural holes.[29,30] It was suggested that the corrugation enhances the catalytic performance of g-C_3N_4 for the selective production of CO/CH_3OH.[30]

In this work, we investigate the interaction between the planar and corrugated g-C_3N_4 with titanium dioxide cluster and clarify the mechanism of the transfer of photogenerated electrons using a combination of different theoretical methods.

Models and computational methods

Models. It is well known that the two main forms of g-C_3N_4 are triazine and heptazine (tri-*s*-triazines), which can simultaneously exist.[31] This work focuses on triazine-based g-C_3N_4, which is used to build corrugated (denoted as cGN) and in planar (denoted as pGN) forms. The idea of studying the corrugated and planar forms of g-C_3N_4 is because the synthesized g-C_3N_4 has a multilayer structure. The surface of g-C_3N_4 can be considered corrugated if the material has a thin structure. In contrast, if the thickness of g-C_3N_4 is thick enough, the surface can be considered planar.

In both, constructed corrugated and planar models, the peripheral atoms were saturated by hydrogen atoms. cGN and pGN consist of 200 atoms and have a molecular formula of $C_{75}N_{100}H_{20}$.

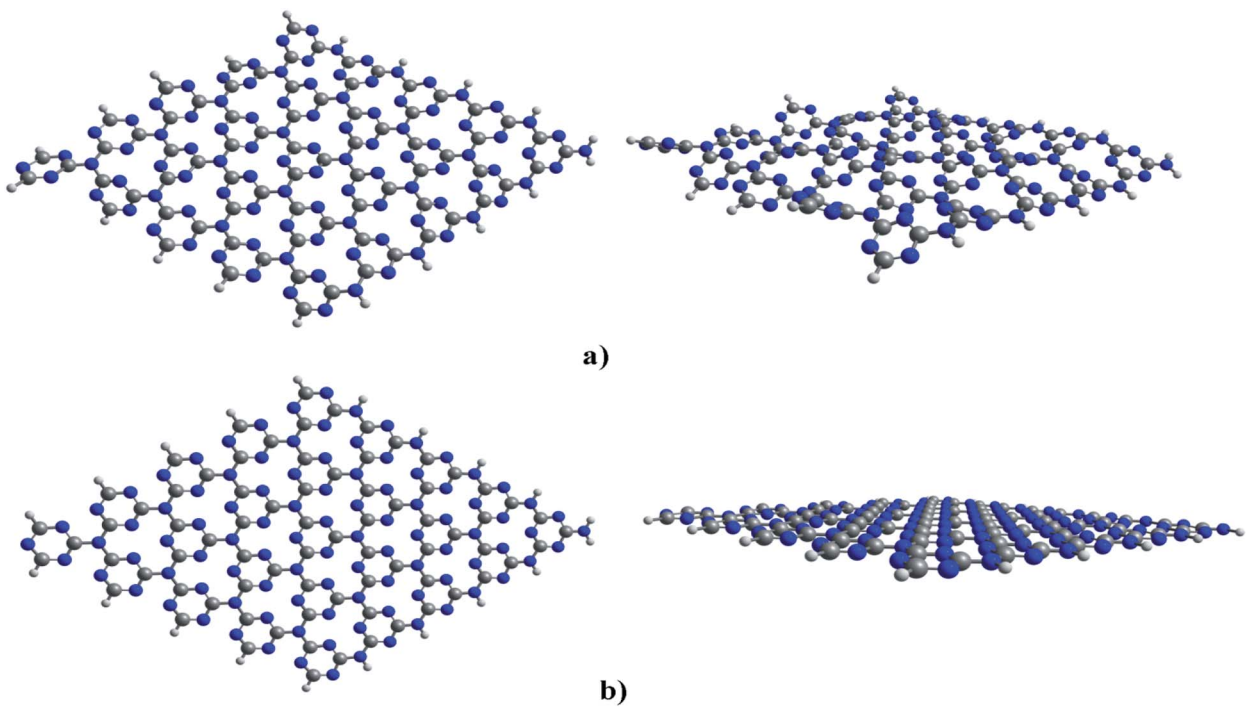

Fig. 1 Optimized structures of cGN (a) and pGN (b); colours: grey-carbon, blue-nitrogen; key distances are in Å.

© 2021 The Author(s). Published by the Royal Society of Chemistry

Open Access Article. Published on 05 May 2021. Downloaded on 2/10/2026 5:16:54 PM.
This article is licensed under a Creative Commons Attribution-NonCommercial 3.0 Unported Licence.

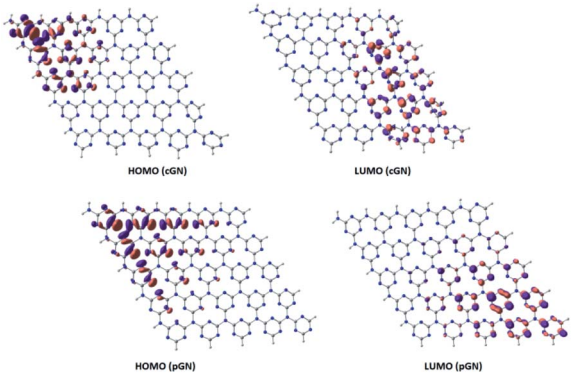

Fig. 2 HOMO and LUMO of cGN (a) and pGN (b) depicted at an isovalue of 0.03 e Å^{-3}.

Titanium dioxide cluster $(TiO_2)_7$ was chosen due to the comparable stability among small $(TiO_2)_n$ clusters (n = 1–9) in terms of cluster formation energy per TiO_2 unit.[32] The initial geometry of the $(TiO_2)_7$ cluster was created from the anatase structure of the bulk.

Computational methods. All optimization and energy calculations were performed using the DFT approach in the generalized gradient approximation (GGA). The PBE (Perdew, Burke, and Ernzerhof) gradient-corrected function was used to calculate the exchange–correlation energy.[33] The double zeta basis plus polarization orbitals (DZP) was used for valence electrons, while core electrons were treated by using norm-conserving pseudopotentials in its fully nonlocal (Kleinman–Bylander) form.[34] The spin-polarized function, which performs a calculation with collinear spin was applied in all calculations, and, thus, the total spin polarization for an optimized structure was automatically determined for the structure with the lowest energy. The calculations have been performed using the SIESTA code.[35]

UV-Vis spectra were calculated using time-dependent-density functional theory (TD-DFT) at CAM-B3LYP/6-31G(d,p) level of theory. This method is implemented in the ORCA code.[36,37] The energy threshold up to which configuration state functions (CSFs) included is 8 eV.

Results and discussions

Electronic structures of cGN, pGN and $(TiO_2)_7$

cGN and pGN. The optimized structures of cGN and pGN are presented in Fig. 1.

The calculated results show that cGN has an energy of 9.2 eV, lower than that of pGN. In other words, cGN is more stable than pGN in terms of the formation energy. The corrugation in the structure of cGN is attributed to the strong repulsion between nitrogen atoms, which are in the sp^2 hybridization state and contain valence electron pairs in the xOy plane.[30] This finding is consistent with previous studies.[29,30]

Analysis of HOMO and LUMO provides useful information about the photogenerated electrons. Fig. 2 illustrates HOMO and LUMO of cGN and pGN. Notably, the multiplicity of both cGN and pGN is 1, implying that the systems do not have unpaired electrons.

The distribution of HOMO and LUMO of cGN and pGN is very similar. In cGN, as well as in pGN, HOMO is mainly located on the nitrogen atoms in the triazine heterocycles (denoted as N1 atoms), while the three-coordinated (linked) nitrogen atoms (denoted as N2 atoms) almost do not contribute to HOMO. The LUMO is primarily supported by N1 and carbon atoms in the heterocycles. It is noted that LUMO is perpendicular to the molecular plane.

When a molecule absorbs light with appropriate energy, electrons can be excited from the occupied molecular orbitals (H) to the unoccupied molecular orbitals (L) to form photo-generated holes (h^+) and electrons (e*), as illustrated in the following scheme:

$$H - e \rightarrow h^+ \quad (1a)$$

$$L + e \rightarrow e^* \quad (1b)$$

Table 1 The parameters of the first excitation of g-C_3N_4

	Excitation energy, eV	Oscillator strength $f \times 10^4$	The amplitude of MO transition		
cGN	4.185	9.93	0.07 (HOMO−4 → LUMO)	0.06 (HOMO−4 → LUMO+3)	0.06 (HOMO−1 → LUMO+1)
pGN	3.769	7.07	0.11 (HOMO−1 → LUMO+12)	0.08 (HOMO → LUMO+22)	0.06 (HOMO → LUMO+15)

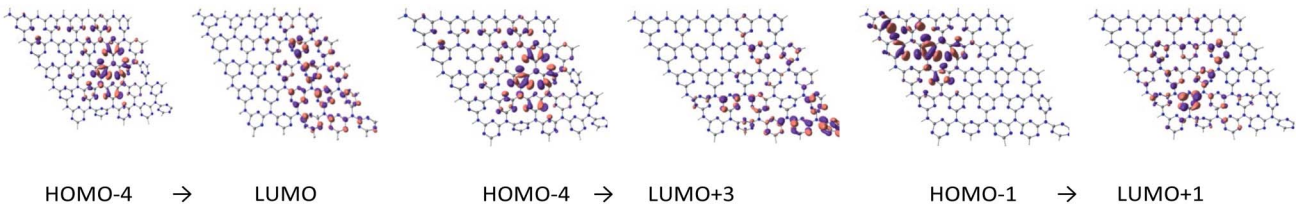

Fig. 3 Molecular orbitals involved in the first excitation of cGN depicted at an isovalue of 0.03 e Å^{-3}.

Open Access Article. Published on 05 May 2021. Downloaded on 2/10/2026 5:16:54 PM.
This article is licensed under a Creative Commons Attribution-NonCommercial 3.0 Unported Licence.

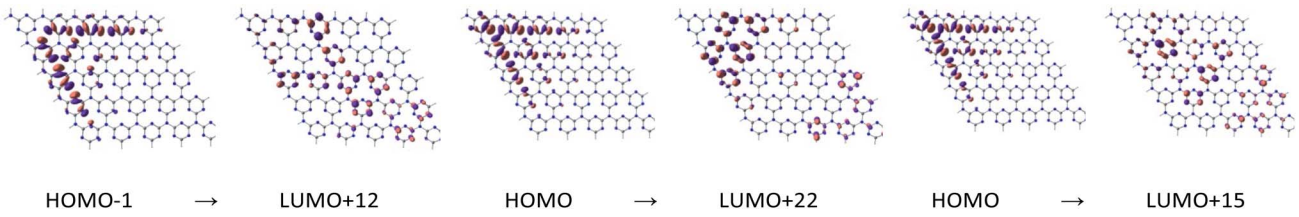

Fig. 4 Molecular orbitals involved in the first excitation of pGN depicted at an isovalue of 0.03 e Å^{-3}.

The h^+–e* pair will play the critical role of an oxidant and a reductant in photocatalysis reactions.

An effective photocatalyst is a material that satisfies the following two requirements: (i) the recombination rate of h^+ and e* is low and (ii) h^+ and e* can be generated under visible light irradiation.

Starting from the first requirement, we propose three hypotheses for the explanation of an effective separation of h^+ and e*:

(i-a): The reduction and oxidation sites are located separately to facilitate photocatalytic reactions,

(i-b): The greater the distance between h^+ and e* is, the more efficient the separation is,

(i-c): The electron density of H (where h^+ is formed) as well as L (where e* is generated) in narrow space results in high densities of h^+ and e*, which would be more effective for the electron transfer process.

The HOMO and LUMO of the cGN system (Fig. 2) are located in different spatial areas and spread across many atoms. As a result, the photogenerated electrons and holes are far apart from each other, leading to their efficient separation and slow recombination. A similar picture is observed for the pGN system. These specific structural features along with the moderate band gap properly contribute to the photocatalytic activity of g-C_3N_4.

To study the nature of the excitation of g-C_3N_4, TD-DFT calculations were performed. The results are summarized in Table 1. Fig. 3 and 4 illustrate molecular orbitals involved in the first excitation of cGN and pGN. The excitation energy of the first excited state was used instead of the bandgap to evaluate the photocatalytic activity. In principle, a photocatalytic process is initiated with the photon absorption of the photocatalyst to generate the first excited state. The calculation results show that cGN has 2070 roots (excitations) and pGN has 2190 roots. The excitation energies of the first excited states of gCN and pCN were determined to be 4.185 eV and 3.769 eV, respectively. It is also noted that the theoretical band gap is strongly dependent on the model size due to the quantum confinement effect.[38,39] Hence, using the energy of the first excited state is meaningful for the same size of the g-C_3N_4 model used.

H and L involved in the first excitation of cGN are distributed in a narrower space than those of pGN. Although the excitation energy of the first excited state of cGN is slightly larger than that of pGN, according to the above-proposed hypothesis (i-c), cGN form is predicted to have higher photocatalytic activities than the pGN form. This finding is consistent with the previous studies.[25,30]

To estimate the photoexcitation probability, fractional occupation density (FOD) was calculated and analyzed. The FOD analysis provides meaningful information about the static correlated electrons, *viz.* active electrons in a molecule.[40,41] The fractional occupation number weighted electron density (ρFOD) at r position is defined as:

$$\rho^{\mathrm{FOD}}(r) = \sum_{i}^{N} (\delta_1 - \delta_2 f_i)|\varphi_i(2)|^2 \quad (2)$$

where φ_i are molecular spin orbitals, f_i is the fractional orbital occupation number ($0 \leq f_i \leq 1$) and the sum is taken over all electronic single-particle levels in the system. The fractional occupation number f_i is calculated as:

$$f_i = \frac{1}{\mathrm{e}^{(\varepsilon_i - E_{\mathrm{F}})/kT_{\mathrm{el}}} + 1} \quad (3)$$

where E_{F} is the Fermi energy level, T_{el} is the electron temperature. The constants δ_1 and δ_2 are chosen to be unity if the level is lower than E_{F}, while they are zero and −1, respectively, for levels higher than E_{F}.[40,41]

The larger the FOD of an atom is, the more active is the atom considered. From the results of FOD calculations for cGN at T_{el} = 12500 K, it can be seen that the nitrogen and carbon atoms in the triazine heterocycles are more active with FOD equal to 0.32 and 0.20 e per bohr^3, respectively. Meanwhile, the linked three coordinated nitrogen atoms outside the ring have a FOD value of only about 0.10 e per bohr^3. These results are consistent with the above-discussed contribution of atoms of g-C_3N_4 into HOMOs and LUMOs. Thus, photoinduced electrons are likely to come from N and C atoms in the heterocycles.

Titanium dioxide $(TiO_2)_7$. Fig. 5 illustrates the HOMO and LUMO of the $(TiO_2)_7$ cluster. Obviously, the HOMO of $(TiO_2)_7$

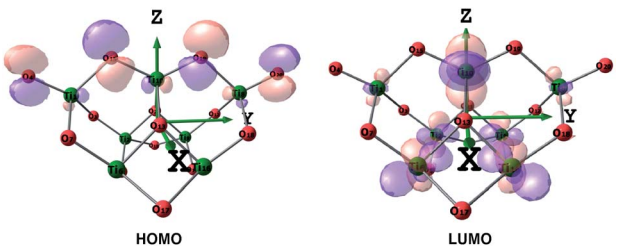

Fig. 5 HOMO and LUMO of the $(TiO_2)_7$ cluster depicted at an isovalue of 0.05 e Å^{-3}, colours: red-oxygen, green-titanium.

© 2021 The Author(s). Published by the Royal Society of Chemistry

Open Access Article. Published on 05 May 2021. Downloaded on 2/10/2026 5:16:54 PM.
This article is licensed under a Creative Commons Attribution-NonCommercial 3.0 Unported Licence.

Table 2 The parameters of the first excitation of $(TiO_2)_7$

	Excitation energy (eV)	Oscillator strength $f \times 10^4$	The amplitude of MO transition		
$(TiO_2)_7$	4.738	7.67	0.88 (HOMO → LUMO)	0.03 (HOMO → LUMO+12)	0.03 (HOMO → LUMO+3)

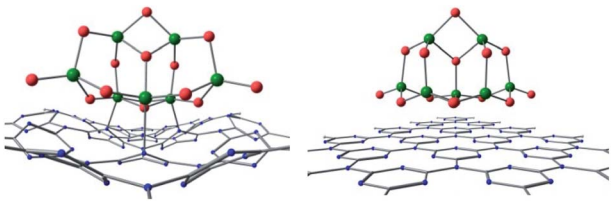

Fig. 6 Optimized structures of the most favorable configurations of cGN/TiO_2 and pGN/TiO_2.

cluster is mainly supported by $2p_z$ orbitals of oxygen atoms with the sum of the squares of the coefficients in the wavefunction's equation was determined to be 0.84. In contrast, the LUMO of $(TiO_2)_7$ cluster was primarily contributed by 3d orbitals of titanium atoms with the sum of the squares of the coefficients in the LUMO's equation equal to 0.70 (considering only 3d orbitals with coefficients larger than 0.10).

Thus, when TiO_2 absorbs photons, electrons will transfer from O atoms contributing to HOMO to Ti atoms, contributing to LUMO. It is noted that in the Frontier HOMO and LUMO of the TiO_2 cluster, contributions of O atoms at different positions to HOMO (and similarly for Ti atoms to LUMO) are different, which is attributed to the different mobility of the atoms.

The excitation energy of the first excited state of $(TiO_2)_7$ is 4.738 eV. The calculation results for the first excited state of $(TiO_2)_7$ are tabulated in Table 2.

Thus, for the $(TiO_2)_7$ cluster, the transition from HOMO to LUMO primarily contributes to the first excitation. Unlike g-C_3N_4, TiO_2 is typically considered chemically inert, *i.e.*, it does not react with other substances and is, therefore, a stable substance that can be used in many different industries and in a variety of applications. This is an important property contributing to the broad practical application of TiO_2. However, the drawback of using anatase in photocatalytic applications lies in its large bandgap. Therefore, the combination of TiO_2 with g-C_3N_4 is expected to decrease the band gap compared to that in pure substances.

Combination of g-C_3N_4 and TiO_2

Interaction between cGN and pGN with $(TiO_2)_7$. When $(TiO_2)_7$ is placed onto the g-C_3N_4 structure, there are a number of possible configurations. In this work, the most favorable configurations for g-C_3N_4/TiO_2 systems were preliminarily determined using the iMTD-GC algorithm, which makes use of extensive metadynamic sampling (MTD), with an additional genetic z-matrix crossing (GC) step at the end. iMTD-GC is implemented in the GFN-xTB (short for "Geometries, Frequencies, and Noncovalent interactions-extended TightBinding") package.[42–44] The generated favorable configurations from iMTD-GC calculations were then fully optimized at GGA-PBE/DZP level of theory. Fig. 6 illustrates the most favorable configurations of cGN and pGN combined with the $(TiO_2)_7$ cluster, which are denoted as cGN/TiO_2 and pGN/TiO_2, respectively.

The interaction between cGN and pGN with $(TiO_2)_7$ cluster is characterized by the interaction energy ($\Delta_{int}E$), which is defined as follows:

$$\Delta_{int}E = E(gC_3N_4/TiO_2) - E(gC_3N_4) - E(TiO_2)$$

The interaction energy determined for cGN/TiO_2 and pGN/TiO_2 was −355.9 kJ mol^{-1} and −185.0 kJ mol^{-1}, respectively. Thus, the formation of g-C_3N_4/TiO_2 systems is energetically favorable. To evaluate the nature of the interaction between g-C_3N_4 and TiO_2 cluster, Mayer bond order (BO) was calculated and analyzed using the following definition:

$$BO(AB) = \sum_{\mu\in A}\sum_{\mu\in B}[(PS)_{\mu\nu} + (PS)_{\nu\mu} + (RS)_{\mu\nu}(RS)_{\nu\mu}]$$

where, P is the total electron density matrix, R is the spin-density matrix and S is the overlap matrix.

The computed BO, distances between atoms (d) and Hirshfeld net atomic charge (q) for cGN/TiO_2 and pGN/TiO_2 are presented in Table 3.

It can be seen that, for the cGN/TiO_2 combination, the distances between Ti and N atoms are slightly larger than the sum of the atomic radius of Ti and N (2.05 Å). This finding is consistent with the reasonable values of BO between Ti atoms and N atoms, which are smaller than 1. A significant charge transfer from cGN to $(TiO_2)_7$ is observed. Thus, the interaction between cGN and TiO_2 clusters is considered to have a chemical nature.

Table 3 Calculation results for cGN/TiO_2 and pGN/TiO_2

Parameters	cGN/TiO_2	pGN/TiO_2
BO	BO(Ti1–N) = 0.386 BO(Ti2–N) = 0.384 BO(Ti3–N) = 0.362	BO(Ti–N) = 0.015–0.071 BO*(Ti–N) = 0.183
d, Å	d(Ti1–N) = 2.235 d(Ti1–N) = 2.243 d(Ti1–N) = 2.327	d(Ti–N) = 3.200
$q(TiO_2)_7$, e	−1.019	−0.741

Open Access Article. Published on 05 May 2021. Downloaded on 2/10/2026 5:16:54 PM.
This article is licensed under a Creative Commons Attribution-NonCommercial 3.0 Unported Licence.

Table 4 Parameters of the first excitation of cGN/TiO_2 and pGN/TiO_2

	Excitation energy (eV)	Oscillator strength $f \times 10^4$	The amplitude of MO transition		
cGN/TiO_2	3.712	7.67	0.34 (HOMO → LUMO+1)	0.10 (HOMO−7 → LUMO+1)	0.08 (HOMO−6 → LUMO+1)
pGN/TiO_2	2.206	2.25	0.16 (HOMO−5 → LUMO)	0.15 (HOMO−3 → LUMO)	0.11 (HOMO−2 → LUMO)

For the pGN/TiO_2 combination, the minimum distance between Ti atoms of the TiO_2 cluster and N atoms of g-C_3N_4 was determined to be 3.2 Å, which is significantly larger than the sum of the atomic radii of Ti and N. The BO between Ti and N atoms is quite small and ranges from 0.015 to 0.071 and the total BO between Ti and N atoms is only 0.183. The charge transfer from pGN to $(TiO_2)_7$ is less than from cGN to $(TiO_2)_7$. Therefore, it can be suggested that the interaction between the TiO_2 cluster and pGN is primarily governed by physical interactions. These findings are in good agreement with the work of Lin *et al.*, who reported that the interaction between g-C_3N_4 and anatase TiO_2 (101) is assigned to the van der Waals heterostructure.[15] This can make the photocatalytic performance of pGN/TiO_2 very different compared to that of the cGN/TiO_2 combination.

Electronic excitation. The excitation energies of the first excited states are 3.712 eV and 2.206 eV for cGN/TiO_2 and pGN/TiO_2, respectively. Table 4 and Fig. 7 illustrate the contribution of molecular orbitals transition to the first excitation of cGN/TiO_2 and pGN/TiO_2.

The calculation results show that the first excitation of cGN/TiO_2 is primarily determined by the transfer of photogenerated electrons from the HOMOs (HOMO, HOMO−7, HOMO−6), mainly located on g-C_3N_4 to the LUMO+1 orbital principally contributed from d orbitals of Ti and $2p_z$ orbitals of N atoms. Electrons from cGN/TiO_2 could be photogenerated by photons with an energy of 3.712 eV, which is much lower than the case of pure cGN and the TiO_2 clusters. Moreover, HOMOs and LUMO+1 orbitals of cGN/TiO_2 are distributed in different spatial areas. When photogenerated electrons are assigned to TiO_2, their density is higher as compared to the distribution of these electrons on the large cGN surface and, thus, makes the electron transfer process more favorable.

The calculated HOMO and LUMO energy levels are −10.575 and −2.406 eV, and, −7.964 and −1.054 eV for the TiO_2 cluster and cGN, respectively. There is an important issue that will be clarified: how do electrons transfer from g-C_3N_4 to TiO_2 when photogenerated? If the interaction between g-C_3N_4 and TiO_2 is just physical, electrons cannot migrate because both g-C_3N_4 and TiO_2 are non-metal. If there is a strong chemical interaction, the electronic structure of each substance will be changed, leading to photocatalytic deactivity.

For the cGN/TiO_2 system, the interaction between TiO_2 and cGN is considered as a weak chemical interaction expressed through a small BO and the atomic distances and, thus, the LUMO+1 orbital of the cGN/TiO_2 system contains both $2p_z$

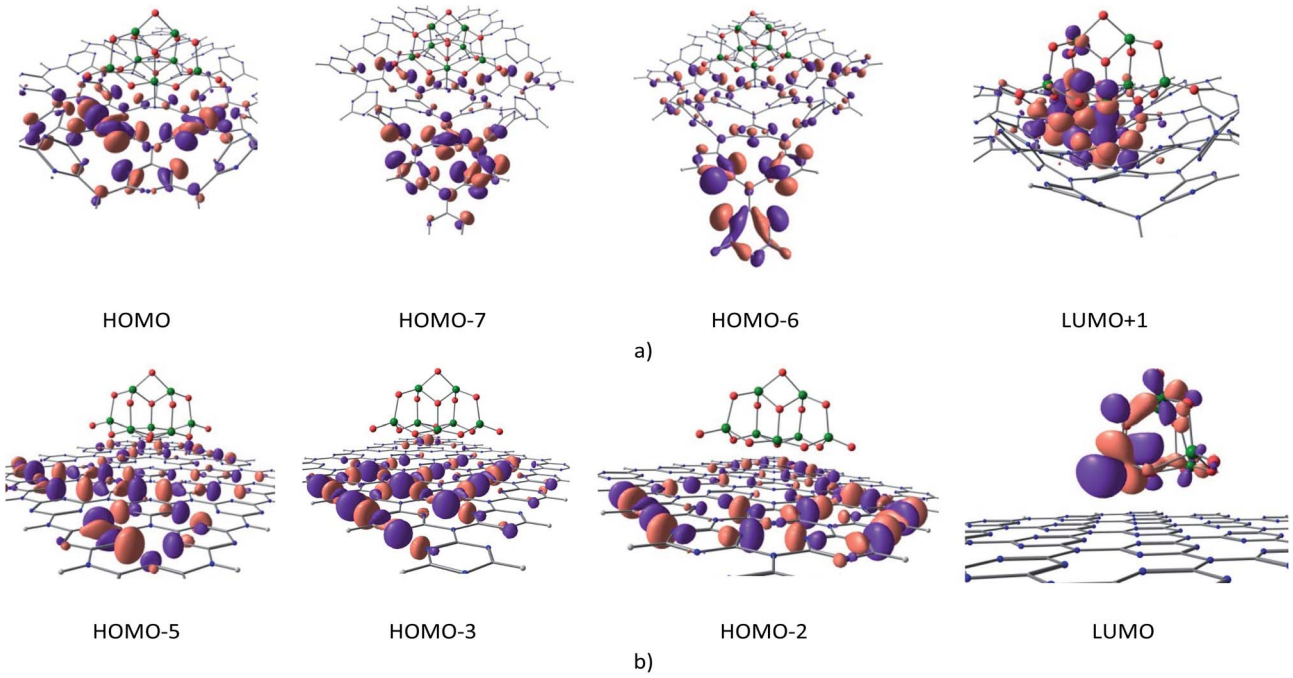

Fig. 7 Molecular orbitals involved in the first excitation of cGN/TiO_2 (a) and pGN/TiO_2 (b) depicted at an isovalue of 0.03 e $Å^{-3}$.

© 2021 The Author(s). Published by the Royal Society of Chemistry

Open Access Article. Published on 05 May 2021. Downloaded on 2/10/2026 5:16:54 PM.
This article is licensed under a Creative Commons Attribution-NonCommercial 3.0 Unported Licence.

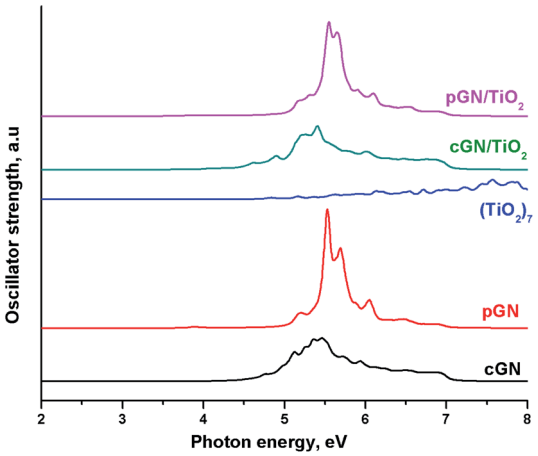

Fig. 8 Calculated UV-Vis spectra of cGN/TiO_2 and pGN/TiO_2.

orbitals of N atoms and 3d orbitals of Ti atoms. Therefore, the electron transition in cGN/TiO_2 can be described as follows: cGN, due to the lower energy of the first excited state as compared to TiO_2, when photogenerated, electrons transfer from the hybrid orbitals containing electron pairs of the N atoms in HOMOs (H) to the $2p_z$ orbitals of N atoms in (LUMO+1) orbitals. This transition is the same as described for g-C_3N_4 (Fig. 2), but the difference is that electrons transfer only to $2p_z$ orbitals of N atoms bound to Ti atoms. Both the $2p_z$ orbitals of N atoms and the 3d orbitals of Ti atoms are involved in the (LUMO+1) orbital, so in this case, the electron transition is almost instantaneous.

For the pGN/TiO_2 system, the LUMO system consists of only orbitals of the TiO_2 cluster. Because there is no chemical interaction between pGN and the TiO_2 cluster, there is no electron transfer from pGN to TiO_2. Thus, for the pGN/TiO_2 system, although the energy of the first excited state is reduced, the photocatalytic efficiency of the combined system is not significantly improved compared to the pure substances.

The calculated UV-Vis spectra for $(TiO_2)_7$, cGN, pGN compared with UV-Vis of cGN/TiO_2 and pGN/TiO_2 are illustrated in Fig. 8. The relative total peak areas (S) in the photon energy region of 2–5 eV for the studied systems are shown in Table 5.

The UV-Vis of pGN/TiO_2 is not different from the parent pGN, proving that there is no chemical interaction between $(TiO_2)_7$ and pGN. Meanwhile, the spectrum of cGN/TiO_2 has a significant shift to the lower energy photon region. This is attributed to the above-mentioned interaction between $(TiO_2)_7$ and cGN. Besides, cGN/TiO_2 exhibits a larger total peak area than that of the pure components and thus, more transitions are appearing in the photon energy region of 2–5 eV. The combination between TiO_2 and cGN improved the light absorption ability of the component due to the synergistic effect. Concerning the idea of using corrugated and planar models of g-C_3N_4 that characterize the thickness of the material (see section Models), our calculation results confirm that exfoliated g-C_3N_4 nanosheets exhibit higher photocatalytic performance than bulk C_3N_4. These findings are in good agreement with the experimental study of Gao *et al.* on the enhancement of the photocatalytic activity of ZnO/g-C_3N_4 composites by regulating the stacked thickness of g-C_3N_4 nanosheets.[45] Their results showed that ZnO/g-C_3N_4 with the middle thickness shows the highest photocatalytic performance.

Table 5 Relative total peak area (S) in the photon energy region of 2–5 eV for $(TiO_2)_7$, cGN, pGN, cGN/TiO_2 and pGN/TiO_2

System	$(TiO_2)_7$	cGN	pGN	cGN/TiO_2	pGN/TiO_2
S	1.0	91.4	32.2	117	38.8

Conclusions

The interactions between planar g-C_3N_4 (pGN) and corrugated g-C_3N_4 (cGN) with the $(TiO_2)_7$ cluster were investigated using the DFT method. The obtained findings show that the cGN chemically interacts with the titanium cluster, while the interaction between pGN and the cluster is assigned to physical nature. The combination of both cGN and pGN with $(TiO_2)_7$ reduces the energy of the first excited state. The photocatalytic activities were estimated based on hypotheses on the location of the reduction and oxidation sites, the distance between the photoinduced holes and electrons and the electron density of the molecular orbitals involved during excitation. cGN/TiO_2 is predicted to have a higher photocatalytic activity than pGN/TiO_2 due to the synergistic effect.

Author contributions

Conceptualization: Nguyen Ngoc Ha; data curation: Nguyen Thi Thu Ha, Pham Thi Be, formal analysis: Nguyen Thi Thu Ha, Phung Thi Lan, Nguyen Thi Mo and Pham Thi Be, investigation: Nguyen Thi Thu Ha, Nguyen Ngoc Ha, Phung Thi Lan, Nguyen Thi Mo and Pham Thi Be; methodology: Nguyen Ngoc Ha, Le Minh Cam and Nguyen Thi Thu Ha; project administration: Nguyen Ngoc Ha; visualization: Phung Thi Lan, Nguyen Thi Mo and Pham Thi Be; writing – original draft: Nguyen Thi Thu Ha, Pham Thi Be, Phung Thi Lan and Nguyen Thi Mo; writing – review & editing: Nguyen Ngoc Ha and Le Minh Cam.

Conflicts of interest

There are no conflicts to declare.

Acknowledgements

This research is funded by Vietnam National Foundation for Science and Technology Development (NAFOSTED) under grant number 05/2018/TN.

Notes and references

1 A. Wang, C. Wang, L. Fu, W. Wong-Ng and Y. Lan, *Nano-Micro Lett.*, 2017, **9**, 1–21.
2 G. Dong, Y. Zhang, Q. Pan and J. Qiu, *J. Photochem. Photobiol., C*, 2014, **20**, 33–50.

Open Access Article. Published on 05 May 2021. Downloaded on 2/10/2026 5:16:54 PM.
This article is licensed under a Creative Commons Attribution-NonCommercial 3.0 Unported Licence.

3 X. Wang, K. Maeda, A. Thomas, K. Takanabe, G. Xin, J. M. Carlsson, K. Domen and M. Antonietti, *Nat. Mater.*, 2009, **8**, 76–80.
4 Z. Chen, S. Zhang, Y. Liu, N. S. Alharbi, S. O. Rabah, S. Wang and X. Wang, *Sci. Total Environ.*, 2020, **731**, 139054.
5 Y. Wei, Q. Zou, P. Ye, M. Wang, X. Li and A. Xu, *Chemosphere*, 2018, **208**, 358–365.
6 P. Wang, S. Sun, X. Zhang, X. Ge and W. Lü, *RSC Adv.*, 2016, **6**, 33589–33598.
7 H. Ma, J. Feng, F. Jin, M. Wei, C. Liu and Y. Ma, *Nanoscale*, 2018, **10**, 15624–15631.
8 S. Ye, R. Wang, M. Z. Wu and Y. P. Yuan, in *Applied Surface Science*, Elsevier B.V., 2015, vol. 358, pp. 15–27.
9 W. J. Ong, L. L. Tan, S. P. Chai and S. T. Yong, *Dalton Trans.*, 2014, **44**, 1249–1257.
10 Y. He, Y. Wang, L. Zhang, B. Teng and M. Fan, *Appl. Catal., B*, 2015, **168–169**, 1–8.
11 J. Wang, C. Qin, H. Wang, M. Chu, A. Zada, X. Zhang, J. Li, F. Raziq, Y. Qu and L. Jing, *Appl. Catal., B*, 2018, **221**, 459–466.
12 S. Wojtyła, K. Śpiewak and T. Baran, *J. Inorg. Organomet. Polym. Mater.*, 2020, **30**, 3418–3428.
13 W. Xing, G. Chen, C. Li, Z. Han, Y. Hu and Q. Meng, *Nanoscale*, 2018, **10**, 5239–5245.
14 X. B. Qian, W. Peng and J. H. Huang, *Mater. Res. Bull.*, 2018, **102**, 362–368.
15 Y. Lin, H. Shi, Z. Jiang, G. Wang, X. Zhang, H. Zhu, R. Zhang and C. Zhu, *Int. J. Hydrogen Energy*, 2017, **42**, 9903–9913.
16 S. Adhikari and D. H. Kim, *Appl. Surf. Sci.*, 2020, **511**, 145595.
17 M. A. Alcudia-Ramos, M. O. Fuentez-Torres, F. Ortiz-Chi, C. G. Espinosa-González, N. Hernández-Como, D. S. García-Zaleta, M. K. Kesarla, J. G. Torres-Torres, V. Collins-Martínez and S. Godavarthi, *Ceram. Int.*, 2020, **46**, 38–45.
18 R. Acharya and K. Parida, *J. Environ. Chem. Eng.*, 2020, **8**, 103896.
19 H. Gao, J. Jia, F. Guo, B. Li, D. Dai, X. Deng, X. Liu, C. Si and G. Liu, *J. Photochem. Photobiol., A*, 2018, **364**, 328–335.
20 J. Liu, B. Cheng and J. Yu, *Phys. Chem. Chem. Phys.*, 2016, **18**, 31175–31183.
21 W. Wang, Y. Liu, J. Qu, Y. Chen, M. O. Tadé and Z. Shao, *ChemPhotoChem*, 2017, **1**, 35–45.
22 R. Fagan, D. E. McCormack, S. J. Hinder and S. C. Pillai, *Materials*, 2016, **9**, 286.
23 B. Zhu, B. Cheng, L. Zhang and J. Yu, *Carbon Energy*, 2019, **1**, 32–56.
24 H. Gao, B. Lu, D. Li, F. Guo, D. Dai, C. Si, G. Liu and X. Zhao, *RSC Adv.*, 2016, **6**, 65315–65321.
25 C. Ren, Y. Zhang, Y. Li, Y. Zhang, S. Huang, W. Lin and K. Ding, *J. Phys. Chem. C*, 2019, **123**, 17296–17305.
26 H. Gao, R. Cao, S. Zhang, H. Yang and X. Xu, *ACS Appl. Mater. Interfaces*, 2019, **11**, 2050–2059.
27 A. Dandia, S. L. Gupta, P. Saini, R. Sharma, S. Meena and V. Parewa, *Curr. Opin. Green Sustain. Chem.*, 2020, **3**, 100039.
28 J. Lei, B. Chen, W. Lv, L. Zhou, L. Wang, Y. Liu and J. Zhang, *Dalton Trans.*, 2019, **48**, 3486–3495.
29 D. T. Vodak, K. Kim, L. Iordanidis, P. G. Rasmussen, A. J. Matzger and O. M. Yaghi, *Chem.–Eur. J.*, 2003, **9**, 4197–4201.
30 L. M. Azofra, D. R. MacFarlane and C. Sun, *Phys. Chem. Chem. Phys.*, 2016, **18**, 18507–18514.
31 L. Zhang, Z. Jin, H. Lu, T. Lin, S. Ruan, X. S. Zhao and Y. J. Zeng, *ACS Omega*, 2018, **3**, 15009–15017.
32 A. Zheng-wang Qu and G.-J. Kroes, *J. Phys. Chem. B*, 2006, **110**(18), 8998–9007.
33 J. P. Perdew, K. Burke and M. Ernzerhof, *Phys. Rev. Lett.*, 1996, **77**, 3865–3868.
34 L. Kleinman and D. M. Bylander, *Phys. Rev. Lett.*, 1982, **48**, 1425–1428.
35 J. M. Soler, E. Artacho, J. D. Gale, A. García, J. Junquera, P. Ordejón and D. Sánchez-Portal, *J. Phys.: Condens. Matter*, 2002, **14**, 2745–2779.
36 F. Neese, *Wiley Interdiscip. Rev.: Comput. Mol. Sci.*, 2012, **2**, 73–78.
37 ORCA Forum – Portal, https://orcaforum.kofo.mpg.de/app.php/portal, accessed 13 February 2021.
38 S. Furukawa and T. Miyasato, *Phys. Rev. B: Condens. Matter Mater. Phys.*, 1988, **38**, 5726–5729.
39 J. Liu, Y. Nie, W. Xue, L. Wu, H. Jin, G. Jin, Z. Zhai and C. Fu, *J. Mater. Res. Technol.*, 2020, **9**, 8020–8028.
40 S. Grimme and A. Hansen, *Angew. Chem., Int. Ed.*, 2015, **54**, 12308–12313.
41 C. A. Bauer, A. Hansen and S. Grimme, *Chem.–Eur. J.*, 2017, **23**, 6150–6164.
42 P. Pracht, F. Bohle and S. Grimme, *Phys. Chem. Chem. Phys.*, 2020, **22**, 7169–7192.
43 S. Grimme, C. Bannwarth and P. Shushkov, *J. Chem. Theory Comput.*, 2017, **13**, 1989–2009.
44 C. Bannwarth, S. Ehlert and S. Grimme, *J. Chem. Theory Comput.*, 2019, **15**, 1652–1671.
45 X. Gao, B. Yang, W. Yao, Y. Wang, R. Zong, J. Wang, X. Li, W. Jin and D. Tao, *Environ. Pollut.*, 2020, **257**, 113577.

© 2021 The Author(s). Published by the Royal Society of Chemistry